Antilocalization of hole carriers in $Pb_{1-x}Eu_xTe$ alloys in the metallic regime

Marcelos L. Peres,* V. A. Chitta, and Nei F. Oliveira, Jr.
Instituto de Física, Universidade de São Paulo, PB 66318, 05315-970 São Paulo, SP, Brazil

D. K. Maude
Grenoble High Magnetic Field Laboratory, Centre National de la Recherche Scientifique, 25 Avenue des Martyrs, 38042 Grenoble, France

P. H. O. Rappl, A. Y. Ueta, and E. Abramof
Laboratório Associado de Sensores e Materiais, Instituto Nacional de Pesquisas Espaciais, PB 515, 12201-970 São José dos Campos, SP, Brazil

(Received 24 September 2008; revised manuscript received 16 December 2008; published 12 February 2009)

Magnetoresistance measurements in *p*-type $Pb_{1-x}Eu_xTe$ alloys, for x varying from 0% up to 5%, have been used to investigate localization and antilocalization effects. These are attributed to both the spin-orbit scattering and to the large Zeeman splitting present in these alloys due to the large values of the effective Landé g factor. The magnetoresistance curves are analyzed using the model of Fukuyama and Hoshino, which takes into account the spin-orbit and Zeeman scattering mechanisms. The spin-orbit scattering time is found to be independent of the temperature, while the inelastic-scattering time increases with decreasing temperature suggesting the electron-phonon interaction as the main scattering mechanism.

DOI: 10.1103/PhysRevB.79.085309 PACS number(s): 05.10.Ln, 05.70.Fh, 05.50.+q

I. INTRODUCTION

PbTe is a narrow gap semiconductor which exhibits interesting properties that differentiate it from other semiconductors.[1–8] It is widely used in detectors and sensor devices operating in the range of visible to infrared radiation. PbTe is a multivalley direct-gap semiconductor with a Fermi surface consisting of four equivalent ellipsoids of revolution with energy minima at the L point of the Brillouin zone. The large dielectric constant[9] ($\varepsilon \sim 1350$ at 4.2K) produces an effective screening against ionized impurities and defects resulting in bulk samples with very high mobility that can exceed 10^2 m^2/V s at low temperatures.[10] The large dielectric constant has also been shown to modify significantly the electron localization and phase breaking mechanisms.[11] In addition, the physics is further enriched by the large value of the Landé g factor and the small effective mass; both of which display considerable anisotropy. Such properties make PbTe an interesting material for possible applications in spintronics. Recently, PbTe was suggested for use as a spin filter[12] since the large value of the Landé g factor should permit such devices to operate at low magnetic fields.

Generally, PbTe films are grown on BaF_2 substrates, regardless of the 4% lattice mismatch between both materials at room temperature. Due to this mismatch, the growth starts nucleating islands and changes to the layer-by-layer mode following the islands coalescence (after ~ 0.1 μm). $PbTe/BaF_2$ films thicker than 3 μm are usually relaxed. At room temperature, the thermal-expansion coefficients of PbTe and BaF_2 are very close ($\sim 2 \times 10^5$ K^{-1}). However, they start to deviate from each other as the temperature is lowered. At 10 K, the thermal-expansion coefficient of BaF_2 is 1 order of magnitude smaller than that of PbTe. Consequently, a tensile strain up to 1.7×10^{-3} can be introduced in the plane of the PbTe film, when cooling the $PbTe/BaF_2$ system from 300 down to 4 K. This strain causes a lifting of the fourfold degeneracy of the L states.[3] Since the films are grown in the [111] direction, the valley with its main axis oriented along this direction (longitudinal valley) is shifted downward in energy by around 5 meV, with respect to the other three oblique valleys.[11] As a consequence, for an *n*-type PbTe film, the three oblique valleys can suffer a depopulation with electrons migrating to the longitudinal valley.[13] In the case of *p*-type samples the inverse occurs, with holes migrating from the longitudinal to the oblique valleys.[4] For high carrier concentrations or high temperatures, all valleys will be occupied, i.e., when the Fermi level is larger than ~ 5 meV.

The introduction of Eu^{2+} ions to form the $Pb_{1-x}Eu_xTe$ alloy drastically changes the optical and electrical properties in the semiconductor.[14] The energy gap increases, while the carrier mobility is reduced, as the Eu content is augmented. The increase in the Eu content also reduces the value of the Landé g factor for holes and electrons.[15] However, this reduction is larger for the conduction band than for the valence band. For this reason, we expect to observe a stronger spin splitting, due to the Zeeman effect ($\sim g\mu_B B$), in *p*-type than in *n*-type samples for a given Eu concentration.

The disorder resulting from the inclusion of Eu ions drastically reduces the carrier mobility through short-range alloy scattering. This disorder also gives rise to a *weak localization*, which results from the quantum interference between the partial carrier wave functions. Weak localization manifests itself at low temperatures as a negative magnetoresistance, which indicates a delocalization of carriers when a weak magnetic field is applied.[16]

In this paper, we present results from magnetotransport measurements on *p*-type $Pb_{1-x}Eu_xTe$ alloys with x varying from 0% up to 5%. All samples present a metallic behavior, except the sample with $x=5\%$, which is on the border of the metal-insulator transition. The measured magnetoresistance curves are characterized by a positive magnetoresistance at

low magnetic fields, which indicate the presence of *antilocalization*, and a negative magnetoresistance at higher fields, indicating the presence of localization. We show that the spin-orbit scattering together with the huge value of the Landé g factors are responsible for the antilocalization effect. Despite the large value of the spin of the Eu^{2+} ions ($S=7/2$), the effect of magnetic scattering is found to be negligible in our samples. To fit the magnetoresistance curves, we use the model developed by Fukuyama and Hoshino[17] that takes into account the Zeeman and spin-orbit contributions to the localization. Fitting our magnetotransport data, we were able to extract the temperature dependence of inelastic- and spin-orbit scattering times.

II. SAMPLE GROWTH

The measurements were performed on films of p-type $Pb_{1-x}Eu_xTe$ with x varying from 0% up to 5%. The samples were grown in a Riber 32P molecular-beam epitaxy (MBE) system onto freshly cleaved (111) BaF_2 substrates. The films were grown at a substrate temperature of 208.5 °C during 2 h, with a deposition rate of 3.9 Å/s, resulting in a 2.8 μm layer thickness. Three effusion cells with PbTe, Eu, and Te_2 were used to grow the samples. Pb (Te) vacancies in PbTe crystals act as acceptors (donors); therefore it is possible to control the concentration and the type of carriers through the chalcogen source flux variation. To provide a p-type sample, an excess of Te_2 was maintained during the growth. The flux rates from the individual effusion cells were measured with an ion gauge, which is mounted on the sample manipulator and can be rotated to the substrate growth position. To obtain crystals with different Eu contents, the ratio between the PbTe and Eu flux rates was varied.

Epitaxial growth on BaF_2 always starts in the three-dimensional Voellmer-Weber mode. However, the coalescence of the PbTe islands starts already at a layer thickness of 100 Å and at 1000 Å a uniform and extremely smooth overlayer has formed.[18] For our samples, which are a few microns thick, we do not expect defects in the thin layer close to the substrate to play a significant role in the electrical transport properties.

III. EXPERIMENTAL RESULTS

For the resistance measurements, a van der Pauw geometry was used. For each sample, an average of the permutations between the contacts was made and the geometric factors f_a and f_b were calculated.[19] The values found are in the range 0.85–0.95 indicating the good quality of the contacts (ideal contacts have $f_a=f_b=1$). For the magnetoresistance measurements, we have averaged over the magnetic field directions using $R_{xx}=[R(B)+R(-B)]/2$ to eliminate any Hall component.

Figure 1 presents the resistance of the p-type $Pb_{1-x}Eu_xTe$ samples normalized at 140 K, for x varying from 0% up to 5%, as a function of the temperature. According to this figure, it is clear that the system behaves like a metal for x values up to 4%, i.e., the resistance decreases as the temperature is lowered. The behavior of the resistance of the $x=5\%$ sample as a function of temperature, which increases and decreases as the temperature is lowered, is an indication that this sample is at the border of the metal-insulator transition.

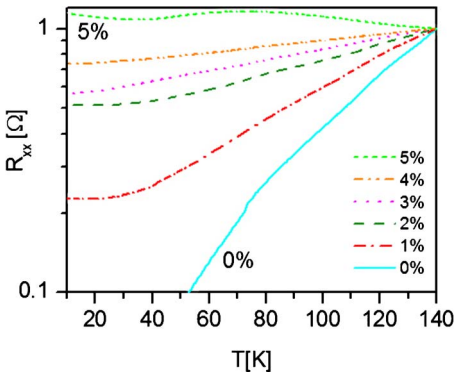

FIG. 1. (Color online) Normalized resistance of the p-type $Pb_{1-x}Eu_xTe$ films (normalized by resistance at 140 K), for x varying from 0% up to 5%, as a function of the temperature.

One can obtain additional information about the conduction regime by analyzing the product k_Fl, where $k_F=(3\pi^2p/N)^{1/3}$ is the Fermi wave number (N is the number of valleys) and $l=\hbar k_F\mu/e$ is the mean-free path. According to the classical Boltzmann conductivity, for $k_Fl\gg1$ the system should behave like a metal. With $k_Fl\sim1$, the system is at the boundary of the metal-insulator transition. For $k_Fl\ll1$, there is no longer diffusion and the system must behave like an insulator. In fact at 10 K, the value of k_Fl for our samples varies from 2836 for $x=0$ down to 0.7 for $x=5\%$. This agrees with the behavior observed in Fig. 1. In Table I we summarize the electrical properties of the samples presented in Fig. 1. The Fermi energy calculated here, assuming a spherical Fermi surface, differs by less than 3% from the value for the anisotropic PbTe Fermi surface calculated from Eq. (14) in Ref. 13. The general trend observed is that the addition of Eu causes a rapid decrease in the mobility and in k_Fl. The hole concentration generally decreases with increasing Eu content, however, there are some fluctuations which may be caused by involuntary variations in the growth conditions or thermal cycling during measurements. Due to the nonsystematic variation in certain parameters with Eu content, care should be taken when comparing results from different samples. However, conclusions drawn for the inelastic- and

TABLE I. Eu concentration x, hole concentration p, carrier mobility μ, product k_Fl, and Fermi energy E_F for the p-type $Pb_{1-x}Eu_xTe$ samples at 10 K.

x (%)	p (m^{-3})	μ (m^2/V s)	k_Fl	E_F (meV)
0	1.2×10^{23}	182	2836	20.6
1	3.1×10^{23}	3.4	99.4	31.8
2	1.1×10^{23}	0.82	11.7	13.5
3	8.1×10^{21}	0.98	2.5	2.1
4	1.6×10^{22}	0.88	3.6	2.8
5	1.3×10^{21}	0.90	0.70	0.5

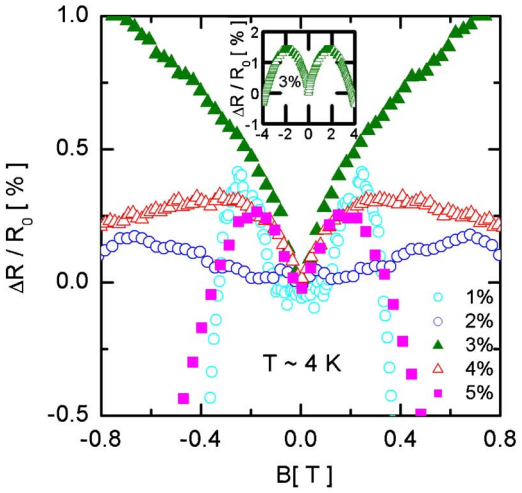

FIG. 2. (Color online) Magnetoresistance at $T=4.2$ K for x varying from 1% up to 5% where weak antilocalization (positive magnetoresistance) and weak localization (negative magnetoresistance) due to quantum interference effects are observed. The inset shows an extended magnetic field range for the sample with $x=3\%$.

spin-orbit scattering times for a given sample remain valid. It is important to note that the Fermi energy is lower than 5 meV for x values higher than 2%. This indicates that for $x=3\%$, 4%, and 5%, only the three oblique valleys contribute to the transport due to the strain effect at low temperatures (see Sec. I).

In order to investigate the transport properties of the p-type $Pb_{1-x}Eu_xTe$ films, we have performed magnetoresistance measurements. The magnetoresistance curves have both a classical contribution ($\sim\mu^2B^2$) and a quantum correction due to the interference of the partial-wave functions of the carriers. To emphasize the quantum corrections of localization and antilocalization, we have subtracted the classical contribution from the experimental data using the mobilities presented in Table I. In addition, any linear Hall component, which is an odd function of the magnetic field, has been removed by averaging the forward and reverse magnetic field data points. The magnetoresistance obtained with this procedure measured at 4.2 K is presented in Fig. 2. For the sample with $x=0$ (not shown), which has a very high mobility, only the classical contribution is observed, since this sample is almost disorder free. The introduction of Eu ions in the system increases the disorder, which enables the observation of the quantum-mechanical interference effects.

For $x=1\%$, a positive magnetoresistance can be observed at low fields, with a maximum at 0.25 T followed by a strong negative magnetoresistance. This indicates that even for low Eu concentrations, the disorder is high enough to cause antilocalization/localization. As the Eu concentration is increased, the maxima in the magnetoresistance shift to higher fields, reaching a maximum for $x=3\%$ at 1.85 T (see inset in Fig. 2). A further increase in the Eu content strongly reduces the carrier mobility, reducing the observed positive magnetoresistance. The sample with $x=5\%$ is closed to a metal-insulator transition and others mechanisms could influence the magnetoresistance. For x values higher than 7% the system lies in the insulating regime, the carriers motion is no longer diffusive, and the transport properties must be analyzed using a more appropriate theory. To be able to analyze the antilocalization/localization, we restrict our studies to samples with low Eu concentration where the system still behaves like a metal.

IV. SCATTERING MECHANISMS AND THEORETICAL MODEL

Since Eu ions have a half-filled $4f$ shell with spin $S=7/2$, spin-disorder scattering might be important in alloys containing Eu ions. In such a situation, the exchange interaction between the spin of the carriers and the Eu-localized magnetic moments could destroy the phase coherence of the partial carrier wave functions, i.e., could change the antilocalization/localization scenario. The spin-disorder scattering can be characterized by two parameters: the spin-flip (τ_s^f) and non-spin-flip (τ_s^z) scattering times.[20] We have estimated τ_s^f and τ_s^z for the sample with $x=4\%$ to verify the effect of the spin-disorder scattering on these alloys using[20]

$$\frac{1}{\tau_s^f}=\frac{1}{2}\frac{2\pi N(E_F)}{\hbar}x\Omega J^2\frac{\alpha/2}{\sinh^2(\alpha/2)}\langle S_z\rangle$$

and

$$\frac{1}{\tau_s^z}=\frac{2\pi N(E_F)}{\hbar}x\Omega J^2\langle S_z^2\rangle,$$

where $N(E_F)$ is the density of states at the Fermi energy, Ω is the average atomic volume, J is the exchange integral, $\alpha=(g\mu_BB)/(k_BT)$, $\langle S_z\rangle=SB_S(S\alpha)$, $\langle S_z^2\rangle=S(S+1)-\langle S_z\rangle\coth(\alpha/2)$, and $B_S(S\alpha)$ is the spin-S Brillouin function. We estimated the scattering times for the sample with $x=4\%$ since it has the highest Eu concentration and is therefore the most likely sample to present spin-disorder scattering, but it is still far enough from the metal-insulator transition region. Using $J=25\times10^{-3}$ eV,[21] $g=14.5$ (for the three oblique valleys in the valence band), we obtain values of around 10^{-10} s for τ_s^f and τ_s^z. These values are 1 to 2 orders of magnitude larger than the inelastic-scattering times obtained from the data analysis presented in Sec. V, indicating that for our samples this mechanism is not important for the scattering process.

Having eliminated spin-dependent scattering, we now consider the contribution of spin-orbit and Zeeman effects to the scattering, using the model proposed by Fukuyama and Hoshino,[17]

$$\frac{\Delta\sigma(B,T)}{A}=\sqrt{h}F\left(\frac{1+t}{h}\right)+\frac{1}{2}\sqrt{\frac{h}{1-\gamma}}\left\{F\left(\frac{t_+}{h}\right)-F\left(\frac{t_-}{h}\right)\right\}-\frac{1}{\sqrt{1-\gamma}}(\sqrt{t_-}-\sqrt{t_+})+\sqrt{t}-\sqrt{t+1},\quad(1)$$

where

$$A=\frac{\sqrt{3}e^2}{2\pi^2l\hbar}\sqrt{\frac{\tau}{\tau_{so}}},\quad h=\left(\frac{l}{l_B}\right)^2\left(\frac{\tau_{so}}{3\tau}\right),\quad t=\frac{\tau_{so}}{4\tau_i},$$

$$\gamma = \left(\frac{1}{2}\frac{g\mu_B B\tau_{so}}{\hbar}\right)^2, \quad t_{\pm} = t + \frac{1}{2}(1 \pm \sqrt{1-\gamma}).$$

l is the mean-free path, $l_B = \sqrt{\hbar/eB}$ is the magnetic length, τ, τ_i, and τ_{so} are the elastic-, inelastic-, and spin-orbit scattering times, respectively. $F(x)$ is Kawabata's[22] function given by

$$F(x) = \sum_{N=0}^{\infty}\left\{2(\sqrt{N+1+x} - \sqrt{N+x}) - \frac{1}{\sqrt{N+\frac{1}{2}+x}}\right\}. \quad (2)$$

The above function [Eq. (2)] can be applied under the conditions

$$\left(\frac{\hbar\omega_c}{E_F}\right) \ll 1, \quad \omega_c\tau \ll 1, \quad \sqrt{\frac{eB}{\hbar}}l \ll 1. \quad (3)$$

According to Eq. (1), the model requires that $\gamma < 1$. The Landé g factor for p-type PbTe is very large ($g_l = 51$ and $g_t = 16$ along and perpendicular to the main ellipsoid axis, respectively). The introduction of the Eu ions modifies the g factor due to the exchange interaction. The longitudinal value g_l decreases, reaching 23.8 for $x = 5\%$, while the transverse value g_t remains approximately constant.[15] These large values for the g factor limit our analysis to low magnetic fields in order to satisfy the condition $\gamma < 1$.

In the case of PbEuTe films, we must consider the contribution of the four valleys to the magnetoresistance. Considering that the contribution from the three oblique valleys are equivalent, we can rewrite Eq. (1) as follows:

$$\Delta\sigma(B,T) = \Delta\sigma_1(B,T) + 3\Delta\sigma_2(B,T). \quad (4)$$

In Eq. (4), $\Delta\sigma_1(B,T)$ is the longitudinal valley contribution and $\Delta\sigma_2(B,T)$ is the contribution of each oblique valley.

V. ANALYSIS AND DISCUSSION

Having established that the magnetic scattering due the Eu ions can be neglected for the p-type PbEuTe samples investigated, we use the model of Fukuyama and Hoshino, which takes into account the spin-orbit and the Zeeman scattering mechanisms, to fit the experimental magnetoresistance data. As an example, we have chosen the sample with $x = 2\%$, since it is far from the insulator region ($k_F l > 1$) and presents localization and antilocalization effects as can be seen in Fig. 2. The fitting was performed using Eq. (4) and the results are presented in Fig. 3(a) for the temperatures in the range 1.4–3.7 K. The conditions described in Eq. (3) are well satisfied until $B \sim 1$ T, but the condition $\gamma < 1$ restricts the fitting to fields below 0.1 T.

Each fitted curve in Fig. 3(a) allows us to extract independently two scattering times: τ_i and τ_{so}. Hence, from the fitting we can obtain the temperature dependence of the scattering times, which is shown in Fig. 3 for the samples with $2\% \leq x \leq 5\%$. In this figure, it is possible to observe that for all samples, τ_i [Fig. 3(b)] increases as the temperature decreases while τ_{so} [Fig. 4(c)] remains almost constant. A deviation from this behavior is observed for the sample with $x = 5\%$ probably due to the fact that this sample is close to the metal-insulator transition. At low temperature, τ_i becomes

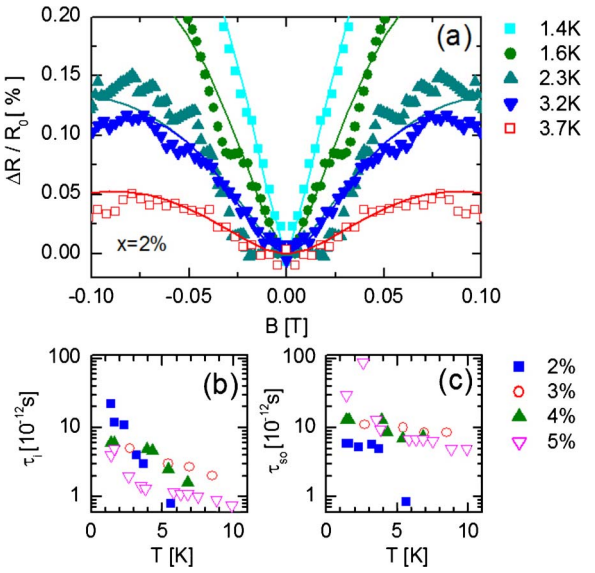

FIG. 3. (Color online) (a) Fitting to the magnetoresistance curves for $x = 2\%$ using Eq. (4). (b) and (c) Extracted inelastic (τ_i) and spin-orbit (τ_{so}) scattering times as a function of the temperature.

longer than τ_{so}, at least for $x = 2\%$. This indicates that the spin-orbit coupling mechanism is dominant and we should observe a positive magnetoresistance enhancement. Indeed, such a behavior is observed in the experimental curves shown in Fig. 3(a). The increase in the inelastic-scattering time (τ_i) as the temperature decreases suggests that the phonon scattering may be the main inelastic-scattering mechanism at low temperatures in p-type $Pb_{1-x}Eu_xTe$ alloys.

The theoretical prediction for electron-phonon scattering is $\tau_i \sim T^{-3}$ for $k_F l \gg 1$ (pure metals) (Refs. 23 and 24) and $\tau_i \sim T^{-2}$ in the presence of disorder $k_F l > 1$.[16] As seen in Fig. 4, for $x = 2\%$, a fitting of τ_i according to $T^{-\alpha}$ gives $\tau_i \sim T^{-2.2}$, which is in good agreement with theory. The slightly larger experimental value obtained for α may be caused by the anisotropy of the valleys. The electron-electron-scattering time is estimated[25] to be $\sim 4.5 \times 10^{-10}$ s so that the main scattering mechanism is due to phonons in our samples.

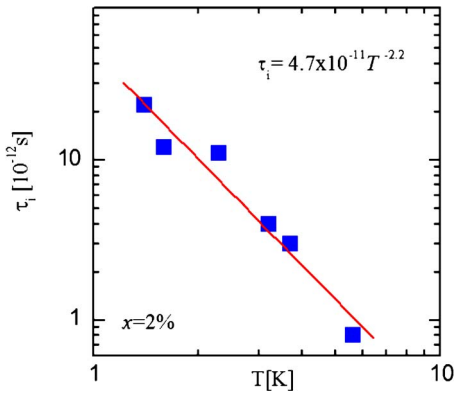

FIG. 4. (Color online) Apparent logarithmic plot of the inelastic-scattering time (τ_i) as a function of temperature for the sample with $x = 2\%$. The dashed line is a linear fit showing the expected $T^{-\alpha}$ law with $\alpha = 2.2$

VI. CONCLUSIONS

We have performed magnetoresistance measurements in p-type $Pb_{1-x}Eu_xTe$ alloys, for x varying from 0% up to 5%. In contrast to electrons in n-type films, the hole carriers in p-type samples exhibit antilocalization effects. This is mainly attributed to the larger effective g factors in p-type samples when Eu magnetic ions are introduced. Even though the Eu ions have a large spin ($S=7/2$), the scattering by magnetic impurities seems to be irrelevant. It is possible to describe the magnetoresistance curve behavior using Fukuyama's model that takes into account the spin-orbit and Zeeman effect scattering mechanisms. The obtained spin-orbit scattering time is independent of the temperature, while the inelastic-scattering time increases as the temperature decreases, suggesting that the main scattering mechanism originates from electron-phonon interaction.

ACKNOWLEDGMENTS

One of the authors (M.L.P.) acknowledges financial support from CNPq. This work has been partially supported by CNRS/FAPESP and CAPES/COFECUB exchange agreements.

*marcelos@if.usp.br

[1] H. Burkhard, G. Bauer, and W. Zawadzki, Phys. Rev. B **19**, 5149 (1979).
[2] A. Krost, B. Harbecke, R. Faymonville, H. Schlegel, E. J. Fantner, K. E. Ambrosch, and G. Bauer, J. Phys. C **18**, 2119 (1985).
[3] J. Singleton, E. Kress-Rogers, A. V. Lewis, R. J. Nicholas, E. J. Fantner, G. Bauer, and A. Otero, J. Phys. C **19**, 77 (1986).
[4] J. Oswald, B. B. Goldberg, G. Bauer, and P. J. Stiles, Phys. Rev. B **40**, 3032 (1989).
[5] B. B. Goldberg, J. E. Furneaux, J. Oswald, G. Bauer, and P. J. Stiles, Semicond. Sci. Technol. **5**, S151 (1990).
[6] S. Yuan, H. Krenn, G. Springholz, and G. Bauer, Phys. Rev. B **47**, 7213 (1993).
[7] J. Oswald, P. Pichler, B. B. Goldberg, and G. Bauer, Phys. Rev. B **49**, 17029 (1994).
[8] V. A. Chitta, W. Desrat, D. K. Maude, B. A. Piot, N. F. Oliveira, Jr., P. H. O. Rappl, A. Y. Ueta, and E. Abramof, Phys. Rev. B **72**, 195326 (2005).
[9] S. Yuan, H. Krenn, G. Springholz, Y. Ueta, G. Bauer, and P. J. McCann, Phys. Rev. B **55**, 4607 (1997).
[10] G. Springholz, G. Bauer, and G. Ihninger, J. Cryst. Growth **127**, 302 (1993).
[11] A. Prinz, G. Brunthaler, Y. Ueta, G. Springholz, G. Bauer, G. Grabecki, and T. Dietl, Phys. Rev. B **59**, 12983 (1999).
[12] G. Grabecki, J. Appl. Phys. **101**, 081722 (2007).
[13] J. R. Burke, B. Houston, and H. T. Savage, Phys. Rev. B **2**, 1977 (1970).
[14] J. A. H. Coaquira, V. A. Chitta, N. F. Oliveira, Jr., P. H. O. Rappl, A. Y. Ueta, E. Abramof, and G. Bauer, J. Supercond. **16**, 115 (2003).
[15] R. C. Patnaik and G. S. Tripathi, Solid State Commun. **112**, 669 (1999).
[16] G. Bergmann, Phys. Rep. **107**, 1 (1984).
[17] H. Fukuyama and K. Hoshino, J. Phys. Soc. Jpn. **50**, 2131 (1981).
[18] G. Springholz, A. Y. Ueta, N. Frank, and G. Bauer, Appl. Phys. Lett. **69**, 2822 (1996).
[19] L. J. van der Pauw, Philips Res. Rep. **13**, 1 (1958).
[20] V. S. Amaral, J. Phys.: Condens. Matter **2**, 8201 (1990).
[21] T. Dietl, C. Sliwa, G. Bauer, and H. Pascher, Phys. Rev. B **49**, 2230 (1994).
[22] A. Kawabata, Solid State Commun. **34**, 431 (1980).
[23] P. Santhanam, S. Wind, and D. E. Prober, Phys. Rev. B **35**, 3188 (1987).
[24] W. E. Lawrence and A. B. Meador, Phys. Rev. B **18**, 1154 (1978).
[25] Z. Ovadyahu, Phys. Rev. Lett. **52**, 569 (1984).